Growth mechanism of star-shaped Au-Ag nanoparticles synthesized by ascorbic acid reduction and underpotential deposition

Yuta Aida[1], Yasuhiro Nakagawa[1], Tetsuo Kishi[1], Masaki Takeguchi[2], Yoshihiro Nemoto[3], Yasutaka Anraku[1], Toshiyuki Ikoma[1]*

1 Department of Materials Science and Engineering, School of Materials and Chemical Technology, Tokyo Institute of Technology, 2-12-1 Ookayama, Meguro-ku, Tokyo, Japan 152-8550

2 Center for Basic Research on Materials, National Institute for Materials Science, 1-2-1 Sengen, Tsukuba, Ibaraki, Japan 305-0047

3 Electron Microscopy Unit, National Institute for Materials Science, 1-2-1 Sengen, Tsukuba, Ibaraki, Japan 305-0047

Corresponding Author

*Corresponding Author: Toshiyuki Ikoma

E-mail: tikoma@ceram.titech.ac.jp

Phone number: +81-3-5734-2519

ABSTRACT

The growth mechanism of star-shaped Au-Ag nanoparticles, which is important for improving the absorption efficiency of nanoparticles in the near-infrared region, remains to be clarified. In this study, the growth mechanism by stabilizing certain facets of Au in spines by underpotential deposition of Ag was investigated. The nanoparticles were analyzed primarily by scanning transmission electron microscopy (STEM) and energy dispersive X-ray spectroscopy. Analysis of spines on nanoparticles synthesized with an Au/Ag ratio of 18/4 revealed that approximately 1 nm of Ag was deposited on the topmost surface of Au, and the growth direction of spines was <200>. Underpotential deposition of Ag nanolayers on specific facets of the spines on nanoparticles was observed for the first time by elemental mapping and high-angle annular dark-field STEM tomography. These findings are expected to contribute to the morphology control of plasmonic nanoparticles.

KEYWORDS, Star-shaped Au-Ag nanoparticles, Growth mechanism, underpotential deposition

1. INTRODUCTION

Synthesis of controlled composition, size, and morphology of plasmonic nanoparticles is of interest for exciting local surface plasmon resonance (LSPR). The most well-known method for synthesizing gold (Au) nanoparticles with anisotropic morphology is the reduction reaction of the aqueous solution in the presence of cetyltrimethylammonium bromide (CTAB); for example, hexagonal nanoplates [1,2], nanoprisms [1–3], nanocube [4] nano-octahedrons [1,4] and nanorod [5–8] can be fabricated depending on the CTAB concentration. The hexagonal nanoplates and nanoprisms grow so that {111} is exposed more than the other aspects from morphological observations using transmission electron microscopy (TEM) [1,3]. Therefore, it has been reported that the mechanism of morphology control is through selective adsorption of CTAB and inhibition of crystal growth on Au{111}, which causes anisotropy in the growth direction, such as only the growth of <110> and <100> [3].

Silver (Ag) ions have also been reported to have a controlling effect on the morphology of plasmonic nanoparticles [9–11]. The morphology control by Ag ions originates from underpotential deposition (UPD) on Au [9,10] and palladium (Pd) [11]. UPD has been described as the electrodeposition of metal monolayer(s) on a foreign metal substrate at potentials that can be significantly less negative than that for deposition on the same metal surface as the adsorbate [12]. In the morphology control of Pd nanoparticles by Ag ions, Ag contributes to stabilization by depositing on {730} of Pd, which forms a morphology consisting of 24 facets indexed as {730} and 8 facets as {111} [11]. On the other hand, a bipyramid-like morphology consisting of {111} and {110} of Au nanoparticles was fabricated by stabilizing Au{110} with Ag ions [9,10]. The Au nanoparticles with high aspect ratio bipyramids was fabricated by increasing the concentration of Ag ions [9,13]. However, the three-dimensional (3D) morphology of nanoparticles with

complex structures using TEM tomography and intensity signal analysis is still less investigated [14].

Star-shaped Au-Ag nanoparticles (AuAgNS) have a unique structure, formed as a result of morphology control by Ag ions on Au. This morphology could shift the frequency of the plasmon resonance to the near-infrared region [15–17]. AuAgNS was fabricated by adding ascorbic acid to a coexisting solution of Ag and Au ions and reducing metal ions [15–17]. The mechanism of growth to star shape was reported to be that the core of Au nanoparticles is first formed by ascorbic acid reduction, then Ag is deposited on the surface by UPD, and the spines having (111) and ($11\bar{1}$) grow along [110] due to the catalytic effect of Ag [15,18]. However, there is no detailed discussion of the stabilization of the crystal plane by UPD of Ag. Furthermore, the distribution of Ag in AuAgNS has not been clarified and the relationship between the core and spines growth orientations has not been sufficiently investigated.

In this study, a novel growth mechanism of AuAgNS was investigated from the TEM analysis of Au and Ag elemental distribution, crystal growth orientation, and three-dimensional (3D) image. In addition, the structure of unique AuAgNS following the high morphological symmetry, such as dodecahedron and icosahedron, of Au nanoparticles reported from computational science was further discussed based on our previous report [17]. These findings contribute to the possibility that plasmonic nanoparticles with unique structures can be controlled to have high absorption efficiency in the near-infrared region.

2. EXPERIMENTAL SECTION

2.1 Material

Hydrogen tetrachloroaurate (III) tetrahydrate ($HAuCl_4 \cdot 3H_2O$), silver nitrate ($AgNO_3$), and L-(+) ascorbic acid were obtained from FUJIFILM Wako Pure Chemical Corp. Ultrapure water (resistivity 18.2 MΩcm) was produced by a Millipore Milli-Q system.

2.2 Synthesis of star-shaped Au-Ag nanoparticles

AuAgNS was synthesized by the method described by Cheng *et al*. [15] with some modifications as in the previously reported paper [17]. The total volume of 10 mM $HAuCl_4$ and 10 mM $AgNO_3$ was fixed at 220 μL. 10 mL of ultrapure water was added to the mixed solution with Au/Ag ratio adjusted to 20/2 or 18/4. Then, 40 μL of 100 mM ascorbic acid solution was added to the diluted Au-Ag solution and stirred for 1 minute. The nanoparticles prepared with an Au/Ag ratio of 20/2 are abbreviated as Au20Ag2, and those with an Au/Ag ratio of 18/4 are as Au18Ag4.

2.3 Characterization method

The optical absorption spectra from 400 nm to 900 nm of the as-prepared nanoparticle solutions were measured using an ultraviolet-visible spectrophotometer (UV-vis, UV-2450, SHIMADZU). The crystalline phase of the samples was identified with an X-ray diffractometer (XRD, X'pert-MPD, PANalytical) using CuKα radiation (λ = 0.15418 nm) at an accelerating voltage of 40 kV and 30 mA. The 2θ range was continuously scanned from 30º to 80º at a rate of 0.6 º/min with a step size of 0.02º. To evaluate the degree of orientation, the Lotgering factor [19] was calculated from the intensity obtained by fitting XRD profiles with a Lorentzian function. When calculating

the Lotgering factor, the intensity data of JSPDS-ICDD: 4-0784 was used as a reference sample. The morphology, selected area electron diffraction (SAED), and elemental distribution of the samples were measured using an aberration-corrected transmission electron microscope (JEM-ARM200F, JEOL) equipped with a cold field emission gun and two silicon drift type energy dispersive X-ray detectors, operated at an accelerating voltage of 200 kV. The samples dispersed into ultrapure water were dropped onto a microgrid and dried in air. SAED was used to analyze the length of the crystal planes and the direction of spine growth. Elemental distribution analysis of Au and Ag by energy dispersive X-ray spectroscopy (EDS) revealed the contribution of Ag to morphology control in AuAgNS. A high-tilt specimen retainer (EM-21311HTR, JEOL) combined with a single-tilt specimen holder (EM-21010, JEOL) was used to acquire a tilt series of high-angle annular dark field (HAADF) scanning transmission electron microscopy (STEM) images from -72 to 72 degrees with every 4 degrees step, followed by STEM-tomography 3D reconstruction using TEMography© (SYSTEM IN FRONTIER INC., Japan).

Changes in absorption spectra during sample synthesis were measured with an ultraviolet-visible spectrometer (UV-vis, UV-2450, SHIMAZU); the wavelength range was from 500 nm to 700 nm, the measurement interval time was 18 seconds, and 100 measurements were conducted. Shifts of the peak tops of UV spectra were discussed with time course dependence for the changes in elemental distribution and morphology.

3. RESULTS AND DISCUSSION

3.1 Formation and structure of star-shaped Au-Ag nanoparticles

Fig. 1 shows the appearance (bluish purple) and optical absorption spectra of the nanoparticle solution. The maximum absorption wavelength (λ_{max}) of Au20Ag2 was 650 nm, and the λ_{max} of Au18Ag4 was 633 nm. As previously reported [17], the difference in λ_{max} is due to the spine length of AuAgNS, indicating that Au20Ag2 has a longer spine compared to Au18Ag4.

Fig. 2 shows XRD patterns of Au20Ag2 and Au18Ag4. Diffractions assigned to Au by JSPDS-ICDD: 4-0784 were confirmed in all samples and no other crystalline phases were identified. The Lotgering factor of Au_{111} calculated from the diffraction intensity was 0.25 for Au20Ag2 and 0.24 for Au18Ag4, suggesting that both samples were slightly oriented to 111, and spines were growing due to the Au deposition of {111}.

Fig. 3 shows the elemental mapping and EDS spectrum of Au20Ag2 or Au18Ag4 analyzed by STEM-EDS. The morphology of both samples, judging from Au mapping, was star-shaped nanoparticles with a core size of approximately 50 nm with high-aspect spines, of which structures were consistent with the previous reports [15–17]. From the Au and Ag mapping of Au20Ag2, only Au was detected at both the core and spines. The EDS spectrum showed an AuMα peak at 2.19 keV, but no Ag peak was detected even though Ag was added during synthesis, meaning that the Ag content would be below the limit of EDS detection. On the other hand, Au18Ag4 exhibited a spine-like structure similar to Au20Ag2 with a spine diameter of less than 10 nm and had a peak of AgLα at 3.02 keV. The elemental mapping showed that Ag existed only on the outermost surface of the AuAgNS. Since the diameter of the spine is less than 10 nm, the electron beam reaches the interior and even the back side, generating characteristic X-rays of the constituent elements.

The thickness of the Ag layer of one spine of Au18Ag4 was analyzed from elemental mapping as shown in Fig. 4. Fig. 4a shows the elemental mapping of Au and Ag. The inset yellow rectangular box where the long side was parallel to the spine slope (the *y*-direction) indicated the analyzed region of characteristic X-ray intensities of Au and Ag. Au and Ag intensities were integrated along the *y*-direction at each distance in the short side (the *x*-direction). Fig. 4b illustrates the intensity plots of Au and Ag against the distance. Interestingly, the intensity curves of Ag and Au were slightly deviated, with Au converging and showing a maximum near the center (6 nm) and Ag having a maximum value at 3.2 nm and attenuating. This suggests that the spine grows conically from the core like epitaxial growth. To analyze the Ag thickness on the outermost surface of the spine, an Au circle with radius r_{Au} and a circle coated with Ag on the outer side with radius r_{Ag} were assumed in Fig. 4b as the cross-section of the spine, and the integral of line segments at each distance was calculated, and fitted and scaled to the intensity plot measured by EDS. The fitted curves of Au and Ag nearly matched the model of the circles with 3.92 nm for r_{Au} and 4.89 nm for r_{Ag}, indicating the Ag thickness on the surface of the spine was 0.97 nm.

Fig. 5 demonstrates the change in absorption spectra measured continuously for 30 minutes every 18 seconds during the synthesis of Au18Ag4. Immediately after adding ascorbic acid in an aqueous solution of dissolved Au^+ and Ag^+ (first measurement), a spectrum with a maximum absorption wavelength of 570 nm, which is associated with the formation of Au nanoparticles without any spines, was observed. After 18 seconds, the maximum absorption wavelength shifted rapidly to the high wavelength side of about 610 nm due to the formation of spines, and then gradually shifted back to 590 nm after stirring for 30 minutes due to the coating of Ag. The blue shift of approximately 20 nm indicates the slow progress of Ag deposition on the nanoparticle surface. Although ascorbic acid cannot normally reduce Ag, it has been suggested that Ag on the

surface of Au can be reduced by UPD [20,21]; Ag^+ ions in the aqueous solution adsorbs as metal Ag atoms like monoatomic layer on the surface of dissimilar metal Au. In other words, while the formation of star-shaped nanoparticles of Au, the deposition of Ag proceeded on specific facets of Au, and Ag nanolayers would be formed.

Fig. 6 shows the STEM images and SAED patterns at the spines of Au18Ag4. The overall morphological symmetry of the spines in the selected Au18Ag4 was not high, which is thought to have been broken during the preparation of the sample. The high-resolution STEM image in Fig. 6b indicates that the twin boundary of Au is observed as a dark line in the angular direction. A *d* value of 0.2355 nm was calculated, corresponding to {111} in a gold unit cell with a face-centered cubic lattice. The result is coincident with the previous reports [15]. In addition, SAED patterns at the spine observed 111 and 002 diffraction spots in both the upper and lower regions across the twin boundary. As shown in Fig. S2 spines grown elsewhere on the nanoparticle also had 111 and 002 diffraction spots and twin boundaries, revealing that the spines grew in a similar manner and in a different direction. The angle of {111} at the upper and lower regions was calculated to be 108 degrees, matching the interior angles of a regular pentagonal. So far, it has been reported that Au forms quintuple twin crystals during deposition from solution [3,13,22]. This suggests that the spines would grow on a quintuple twin of the Au core at the apexes composed of the five triangle facets of the icosahedron.

Fig. 6b shows an analysis of the exposed surface of the upper part, which can be observed along the [110] zone axis. White lines indicate {200} and red lines outline the nanoparticles. The Miller index of the surface has been reported by analyzing the number of atoms on the topmost surface [23–25]; in this paper, the topmost surface of the TEM image is unclear, so the discussion is based on angles. The angle between {200} and the side is 11°, which is almost consistent with 11.42°,

the angle between (200) and (711). Furthermore, the angle between {200} and the tip is 54°, which coincides with 54.74°, the angle between (200) and (111). Therefore, the spines are considered to have a structure consisting of {711} at the sides and {111} at the tip. This indicates that Ag deposition by UPD contributes to the stabilization of facets with high surface energy. Galvanic replacement reactions have also been reported as one of the reactions between Au and Ag [20,26,27]. Galvanic replacement reaction is a reaction in which core Ag is replaced by Au due to ionization tendencies, and has been applied to the synthesis of hollow structures [20,26,27]; however, the contribution to specific surfaces has not been reported. From these results and the discussion of the galvanic replacement reaction, it is considered that the morphology control would be due to UPD.

Three-dimensional (3D) images of Au20Ag2 and Au18Ag4 were produced by HAADF-STEM tomography. Fig. 7 shows a portion of a 3D image of Au18Ag4. Rotation movies of the3D images are included in this paper. The 3D images confirm that Au20Ag2 and Au18Ag4 are nanoparticles with 3D-grown spines. The spines of the nanoparticles were partially broken during preparation and were observed as images with lost symmetry in the orientation of the spines. The color of the 3D image indicates the signal intensity of HAADF-STEM images with blue areas having higher signal intensity than green areas. Fig. 7b shows a green layer on the surface of the blue region. The signal intensity of HAADF-STEM appears as 1.7-2.0 power of the atomic number [28–30]. Thus, the areas indicated by blue in the 3D image are thought to be Au, and the areas shown in green are Ag. Fig. 7b shows only the areas of low signal intensity, suggesting that Ag is present at the uppermost surface of the nanoparticles, since almost no change was observed in the images of Fig. 5a and Fig. 5b. This result is in good agreement with the EDS results.

3.2 Growth mechanism of AuAgNS

Fig. 8 shows a schematic diagram of the novel growth mechanism of AuAgNS. When ascorbic acid is added to an aqueous solution containing both Au^{3+} and Ag^{+} ions, Au^{3+} is first reduced to form Au nucleus. The rapid reduction of Au^{3+} in the presence of Ag^{+} can disturb the crystal symmetry of Au and form nuclei with five-fold pseudosymmetry [31]. After the Au nucleus grow into the icosahedral core, Au {111} grows from the center of the nucleus toward the apex of the triangle. This is consistent with our previous reports [17]. Subsequently, the nanoparticles grow into a star shape due to the ascorbic acid reduction and UPD. Specifically, Ag is deposited on specific facets of Au {711} by UPD, which helps stabilizing Au {711} and causing Au to grow in a spine-like shape. The structure with {111} tip and {711} side is similar to previously reported structures of nanorods with {111} tip and {100} or {110} side [32]. Although morphology control of nanoparticles by UPD has been proposed [10,11,13], no images of Ag deposited on specific facets have been reported so far. In this paper, EDS and STEM images including HAADF-STEM tomography show for the first time that Ag is deposited on the facets with a high surface energy of Au, the side of Au {111}. This suggests that the deposition and stabilization of Ag on specific facets by UPD contribute to morphology control and have a significant effect on plasmonics.

CONCLUSIONS

Star-shaped Au-Ag nanoparticles with different Au/Ag ratios were synthesized by mixing a reducing agent, ascorbic acid, into a solution containing both Au^{3+} and Ag^{+} ions. As the growth mechanism of the nanoparticles, based on the angle of {111} in the twin spine of 108°, the quintuple twin of Au core with the icosahedron having the twin boundary was formed, and the spine grew epitaxially from the apex of the icosahedron core in <200>. From the results of STEM, EDS, SAED, and HAADF-STEM tomography, Ag adsorbed to a specific Au facet by UPD, stabilized the facets with high surface energy, and formed an Ag nanolayer with a thickness of less than 1 nm. It is the first observation of Ag deposited on the outermost surface of nanoparticles by UPD. These findings are expected to contribute to further advances in the morphology control of plasmonic nanoparticles.

Acknowledgments

This work was supported by NIMS microstructural characterization platform as a program of "Nanotechnology Platform" of the Ministry of Education, Culture, Sports, Science and Technology (MEXT), Japan, Grant Number A-21-NM-0080. This work was also supported by Grant-in-Aid for Scientific Research(C) (23K11845) from the Japan Society for the Promotion of Science.

ABBREVIATIONS

LSPR, local surface plasmon resonance; TEM, transmission electron microscopy; STEM, scanning transmission electron microscopy; HAADF, high-angle annular dark field; SAED, selected area electron diffraction; EDS, energy dispersive X-ray spectroscopy; UPD, underpotential deposition; UV-vis, ultraviolet-visible; XRD, X-ray diffraction

REFERENCES

[1] Y. Huang, W. Wang, H. Liang, H. Xu, Surfactant-promoted reductive synthesis of shape-controlled gold nanostructures, Cryst. Growth Des. 9 (2009) 858–862. https://doi.org/10.1021/cg800500c.

[2] M. Kasture, M. Sastry, B.L.V. Prasad, Halide ion controlled shape dependent gold nanoparticle synthesis with tryptophan as reducing agent: Enhanced fluorescent properties and white light emission, Chem. Phys. Lett. 484 (2010) 271–275. https://doi.org/10.1016/j.cplett.2009.11.052.

[3] T.H. Ha, H.J. Koo, B.H. Chung, Shape-controlled syntheses of gold nanoprisms and nanorods influenced by specific adsorption of halide ions, J. Phys. Chem. C. 111 (2007) 1123–1130. https://doi.org/10.1021/jp066454l.

[4] B.S. Yin, J.Q. Hu, S.Y. Ding, A. Wang, J.R. Anema, Y.F. Huang, Z.C. Lei, D.Y. Wu, Z.Q. Tian, Identifying mass transfer influences on Au nanoparticles growth process by centrifugation, Chem. Commun. 48 (2012) 7353–7355. https://doi.org/10.1039/c2cc32491a.

[5] W. Hu, Wiria, W.L. Ong, G.W. Ho, High yield shape control of monodispersed Au nanostructures with 3D self-assembly ordering, Colloids Surfaces A Physicochem. Eng. Asp. 358 (2010) 108–114. https://doi.org/10.1016/j.colsurfa.2010.01.029.

[6] C. Morasso, S. Picciolini, D. Schiumarini, D. Mehn, I. Ojea-Jiménez, G. Zanchetta, R. Vanna, M. Bedoni, D. Prosperi, F. Gramatica, Control of size and aspect ratio in

hydroquinone-based synthesis of gold nanorods, J. Nanoparticle Res. 17 (2015). https://doi.org/10.1007/s11051-015-3136-9.

[7] R.N. Moussawi, D. Patra, Synthesis of Au Nanorods through Prereduction with Curcumin: Preferential Enhancement of Au Nanorod Formation Prepared from CTAB-Capped over Citrate-Capped Au Seeds, J. Phys. Chem. C. 119 (2015) 19458–19468. https://doi.org/10.1021/acs.jpcc.5b04447.

[8] J. Liu, J.N. Duggan, J. Morgan, C.B. Roberts, Seed-mediated growth and manipulation of Au nanorods via size-controlled synthesis of Au seeds, J. Nanoparticle Res. 14 (2012). https://doi.org/10.1007/s11051-012-1289-3.

[9] T.T. Tran, X. Lu, Synergistic effect of Ag and Pd ions on shape-selective growth of polyhedral Au nanocrystals with high-index facets, J. Phys. Chem. C. 115 (2011) 3638–3645. https://doi.org/10.1021/jp111997s.

[10] Y. Qin, Y. Lu, D. Yu, J. Zhou, Controllable synthesis of Au nanocrystals with systematic shape evolution from an octahedron to a truncated ditetragonal prism and rhombic dodecahedron, CrystEngComm. 21 (2019) 5602–5609. https://doi.org/10.1039/c9ce01022j.

[11] N.S.R. Satyavolu, A.S. Peinetti, Y. Wang, A.S. Ali, J.W. Lin, Y. Lu, Silver-Assisted Synthesis of High-Indexed Palladium Tetrahexahedral Nanoparticles and Their Morphological Variants, Chem. Mater. 31 (2019) 2923–2929. https://doi.org/10.1021/acs.chemmater.9b00275.

[12] E. Herrero, L.J. Buller, H.D. Abruña, Underpotential deposition at single crystal surfaces of Au, Pt, Ag and other materials, Chem. Rev. 101 (2001) 1897–1930. https://doi.org/10.1021/cr9600363.

[13] M. Liu, P. Guyot-Sionnest, Mechanism of silver(I)-assisted growth of gold nanorods and bipyramids, J. Phys. Chem. B. 109 (2005) 22192–22200. https://doi.org/10.1021/jp054808n.

[14] A. Skorikov, W. Albrecht, E. Bladt, X. Xie, J.E.S. Van Der Hoeven, A. Van Blaaderen, S. Van Aert, S. Bals, Quantitative 3D Characterization of Elemental Diffusion Dynamics in Individual Ag@Au Nanoparticles with Different Shapes, ACS Nano. 13 (2019) 13421–13429. https://doi.org/10.1021/acsnano.9b06848.

[15] L.C. Cheng, J.H. Huang, H.M. Chen, T.C. Lai, K.Y. Yang, R.S. Liu, M. Hsiao, C.H. Chen, L.J. Her, D.P. Tsai, Seedless, silver-induced synthesis of star-shaped gold/silver bimetallic nanoparticles as high efficiency photothermal therapy reagent, J. Mater. Chem. 22 (2012) 2244–2253. https://doi.org/10.1039/c1jm13937a.

[16] J. Krajczewski, K. Kołątaj, S. Pietrasik, A. Kudelski, Silica-covered star-shaped Au-Ag nanoparticles as new electromagnetic nanoresonators for Raman characterisation of surfaces, Spectrochim. Acta - Part A Mol. Biomol. Spectrosc. 193 (2018) 1–7. https://doi.org/10.1016/j.saa.2017.11.060.

[17] Y. Aida, Y. Nakagawa, T. Kishi, T. Ikoma, Optical Absorption Spectra of Star-Shaped Au–Ag Nanoparticles by Discrete Dipole Approximation Calculation Considering Highly

Symmetrical Models, Plasmonics. 18 (2023) 299–310. https://doi.org/10.1007/s11468-022-01764-y.

[18] E.A. Kwizera, E. Chaffin, X. Shen, J. Chen, Q. Zou, Z. Wu, Z. Gai, S. Bhana, R. Oconnor, L. Wang, H. Adhikari, S.R. Mishra, Y. Wang, X. Huang, Size- and shape-controlled synthesis and properties of magnetic-plasmonic core-shell nanoparticles, J. Phys. Chem. C. 120 (2016) 10530–10546. https://doi.org/10.1021/acs.jpcc.6b00875.

[19] F.K. Lotgering, Topotactical reactions with ferrimagnetic oxides having hexagonal crystal structures-I, J. Inorg. Nucl. Chem. 9 (1959) 113–123. https://doi.org/10.1016/0022-1902(59)80070-1.

[20] Y. Yang, J. Liu, Z.W. Fu, D. Qin, Galvanic replacement-free deposition of au on ag for core-shell nanocubes with enhanced chemical stability and SERS activity, J. Am. Chem. Soc. 136 (2014) 8153–8156. https://doi.org/10.1021/ja502472x.

[21] W. He, X. Wu, J. Liu, X. Hu, K. Zhang, S. Hou, W. Zhou, S. Xie, Design of AgM bimetallic alloy nanostructures (M = Au, Pd, Pt) with tunable morphology and peroxidase-like activity, Chem. Mater. 22 (2010) 2988–2994. https://doi.org/10.1021/cm100393v.

[22] X. Liang, Y. Yang, C. Zou, W. Chen, H.X. Zou, Y. Yang, Au decahedra with High yield for the improved synthesis of Au nanobipyramids, Colloids Surfaces A Physicochem. Eng. Asp. 597 (2020) 124749. https://doi.org/10.1016/j.colsurfa.2020.124749.

[23] H.E. Lee, K.D. Yang, S.M. Yoon, H.Y. Ahn, Y.Y. Lee, H. Chang, D.H. Jeong, Y.S. Lee, M.Y. Kim, K.T. Nam, Concave Rhombic Dodecahedral Au Nanocatalyst with Multiple

High-Index Facets for CO2 Reduction, ACS Nano. 9 (2015) 8384–8393. https://doi.org/10.1021/acsnano.5b03065.

[24] L. Li, Y. Peng, Y. Yue, Y. Hu, X. Liang, P. Yin, L. Guo, Synthesis of concave gold nanocuboids with high-index facets and their enhanced catalytic activity, Chem. Commun. 51 (2015) 11591–11594. https://doi.org/10.1039/c5cc02106e.

[25] Y. Song, T. Miao, P. Zhang, C. Bi, H. Xia, D. Wang, X. Tao, {331}-Faceted trisoctahedral gold nanocrystals: Synthesis, superior electrocatalytic performance and highly efficient SERS activity, Nanoscale. 7 (2015) 8405–8415. https://doi.org/10.1039/c5nr01049g.

[26] Y. Sun, Y. Xia, Mechanistic study on the replacement reaction between silver nanostructures and chloroauric acid in aqueous medium, J. Am. Chem. Soc. 126 (2004) 3892–3901. https://doi.org/10.1021/ja039734c.

[27] J. Chen, F. Saeki, B.J. Wiley, H. Cang, M.J. Cobb, Z.Y. Li, L. Au, H. Zhang, M.B. Kimmey, X. Li, Y. Xia, Gold nanocages: Bioconjugation and their potential use as optical imaging contrast agents, Nano Lett. 5 (2005) 473–477. https://doi.org/10.1021/nl047950t.

[28] E. Abe, Atomic-Scale Characterization of Nanostructured Metallic Materials by HAADF/Z-contrast STEM, Mater. Trans. 44 (2003) 2035–2041. https://doi.org/10.2320/matertrans.44.2035.

[29] P.M. Voyles, Imaging single atoms with Z-contrast scanning transmission electron microscopy in two and three dimensions, Microchim. Acta. 155 (2006) 5–10. https://doi.org/10.1007/s00604-006-0500-6.

[30] K. Sader, A. Brown, R. Brydson, A. Bleloch, Quantitative analysis of image contrast in phase contrast STEM for low dose imaging, Ultramicroscopy. 110 (2010) 1324–1331. https://doi.org/10.1016/j.ultramic.2010.06.008.

[31] X. Li, X. Lin, X. Zhao, H. Wang, Y. Liu, S. Lin, L. Wang, S. Cong, Self-assembled monolayer film of concave star-shaped Au nanocrystals as highly efficient SERS substrates, Appl. Surf. Sci. 518 (2020) 146217. https://doi.org/10.1016/j.apsusc.2020.146217.

[32] C.J. Johnson, E. Dujardin, S.A. Davis, C.J. Murphy, S. Mann, Growth and form of gold nanorods prepared by seed-mediated, surfactant-directed synthesis, J. Mater. Chem. 12 (2002) 1765–1770. https://doi.org/10.1039/b200953f.

Table and Figure captions

Fig. 1 Appearance of nanoparticle solutions and optical absorption spectra; (a) Au20Ag2, (b) Au18Ag4.

Fig. 2 XRD patterns of (a) Au20Ag2 and (b) Au18Ag4.

Fig. 3 Elemental distribution maps (a, c) and EDS spectra (b, d) of Au20Ag2 (a, b) and Au18Ag4 (c, d).

Fig. 4 Ag Layer analysis in spine; (a) elemental distribution and analytical range of spines. (b) Ag layer thickness calculated by fitting from EDS signal intensity.

Fig. 5 Change over time of the absorption spectrum of Au18Ag4 during synthesis.

Fig. 6 STEM images of Au18Ag4; (a) whole image, (b) enlarged image of spines, and (c) SAED patterns of upper grain boundary.

Fig. 7 Tomography of Au18Ag4; (a) overall view, (b) image with low-signal area extracted.

Fig. 8 Schematic diagram of the novel growth mechanism of star-shaped nanoparticles; red is Au atom and green is Ag.

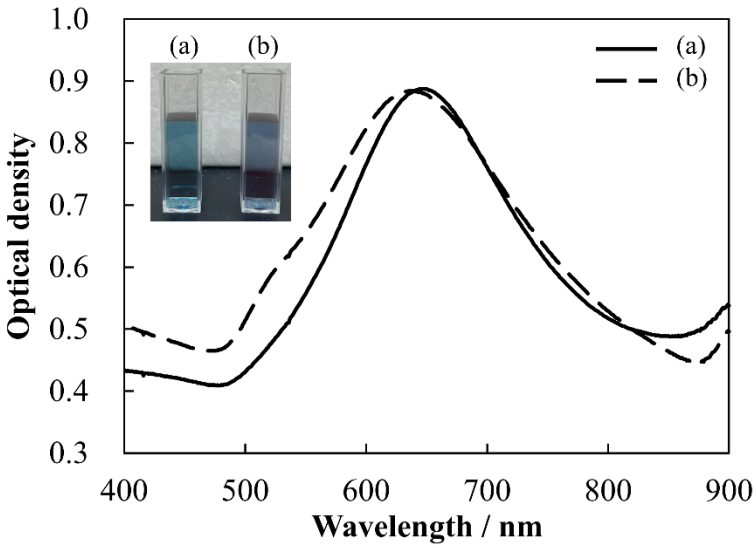

Fig. 1 Appearance of nanoparticle solutions and optical absorption spectra; (a) Au20Ag2, (b) Au18Ag4.

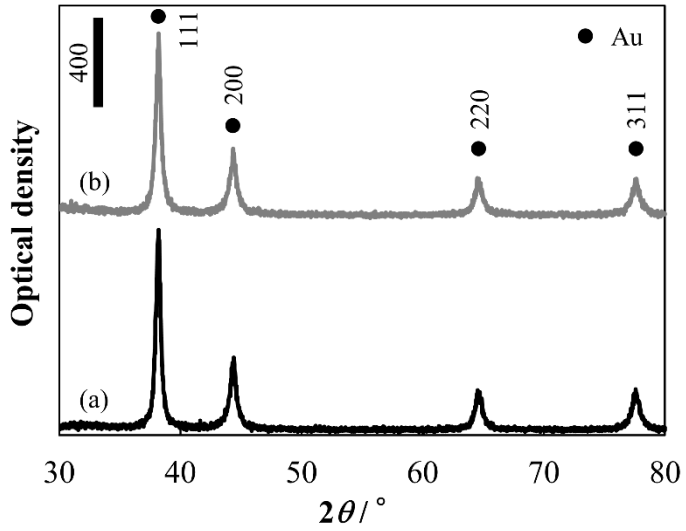

Fig. 2 XRD patterns of (a) Au20Ag2 and (b) Au18Ag4.

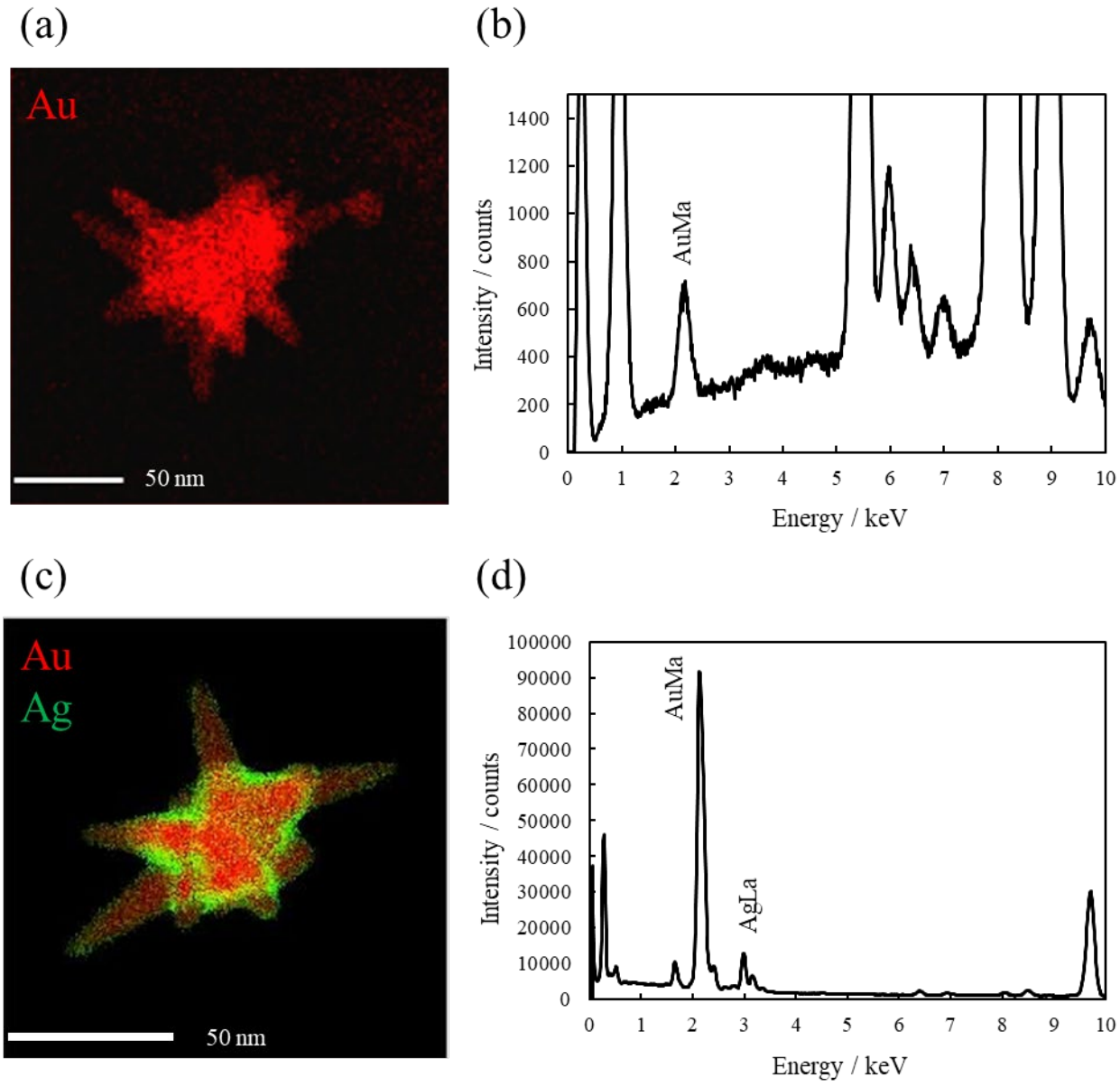

Fig. 3 Elemental distribution maps (a, c) and EDS spectra (b, d) of Au20Ag2 (a, b) and Au18Ag4 (c, d).

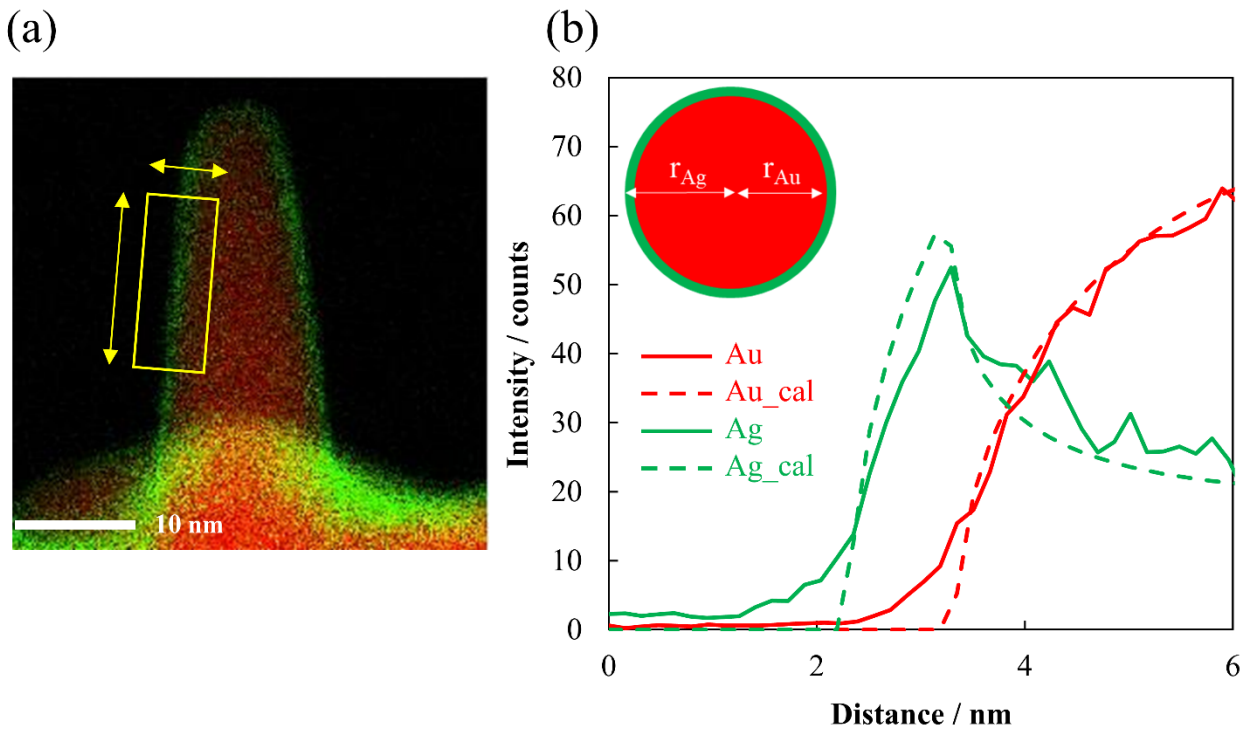

Fig. 4 Ag layer analysis in Spine; (a) elemental distribution and analytical range of spines. (b) Ag layer thickness calculated by fitting from EDS signal intensity.

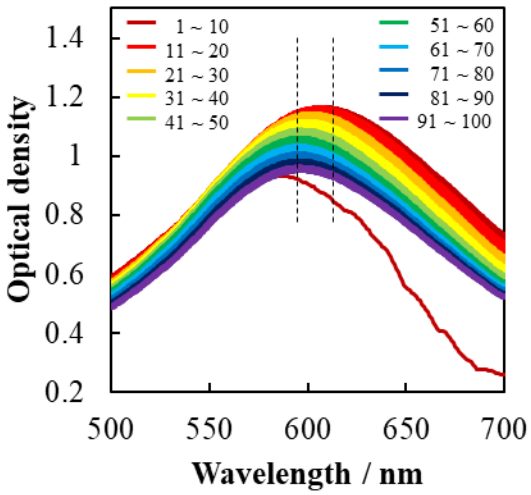

Fig. 5 Change over time of the absorption spectrum of Au18Ag4 during synthesis.

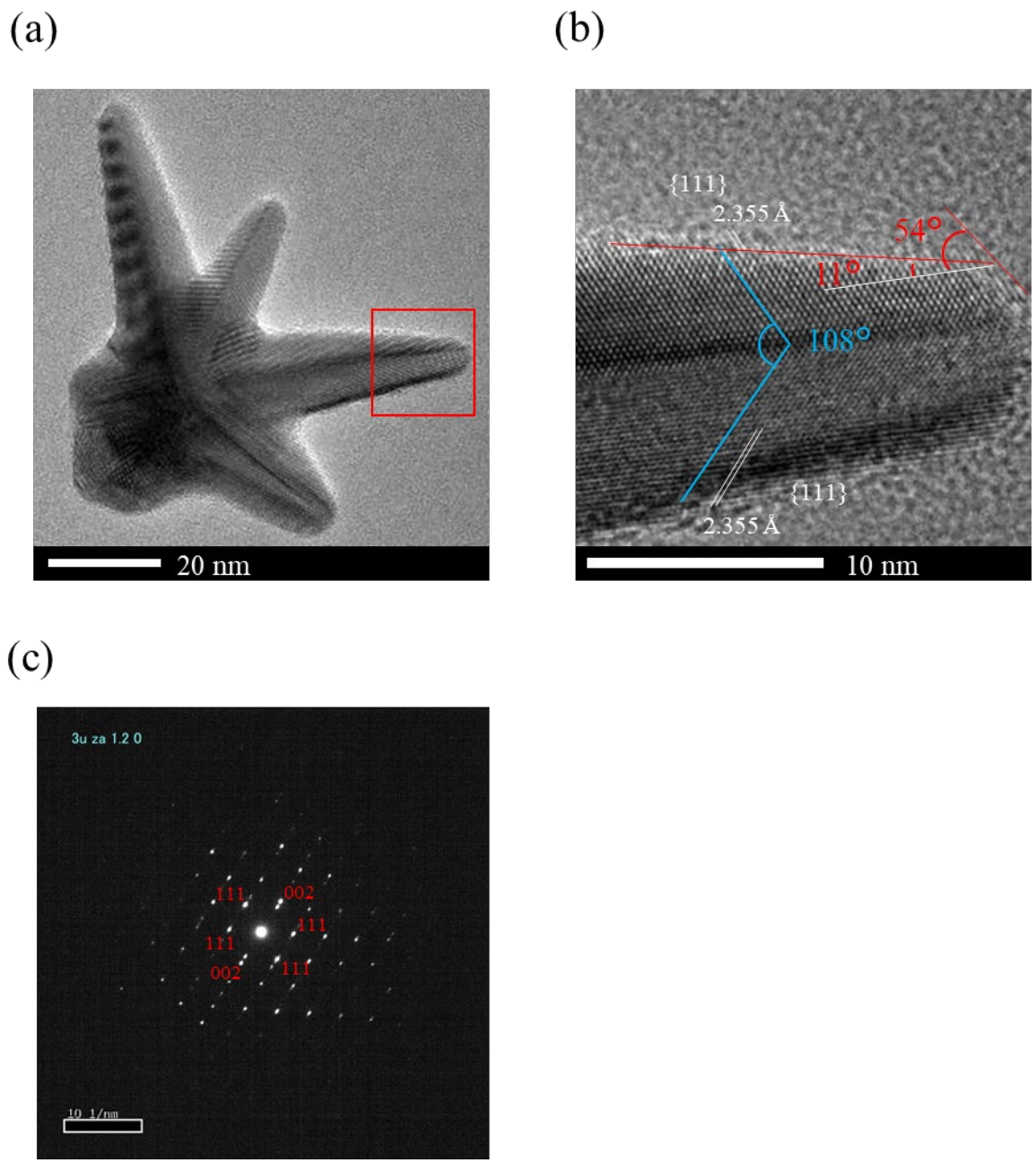

Fig. 6 STEM images of Au18Ag4; (a) whole image, (b) enlarged image of spines, and (c) SAED patterns of upper grain boundary.

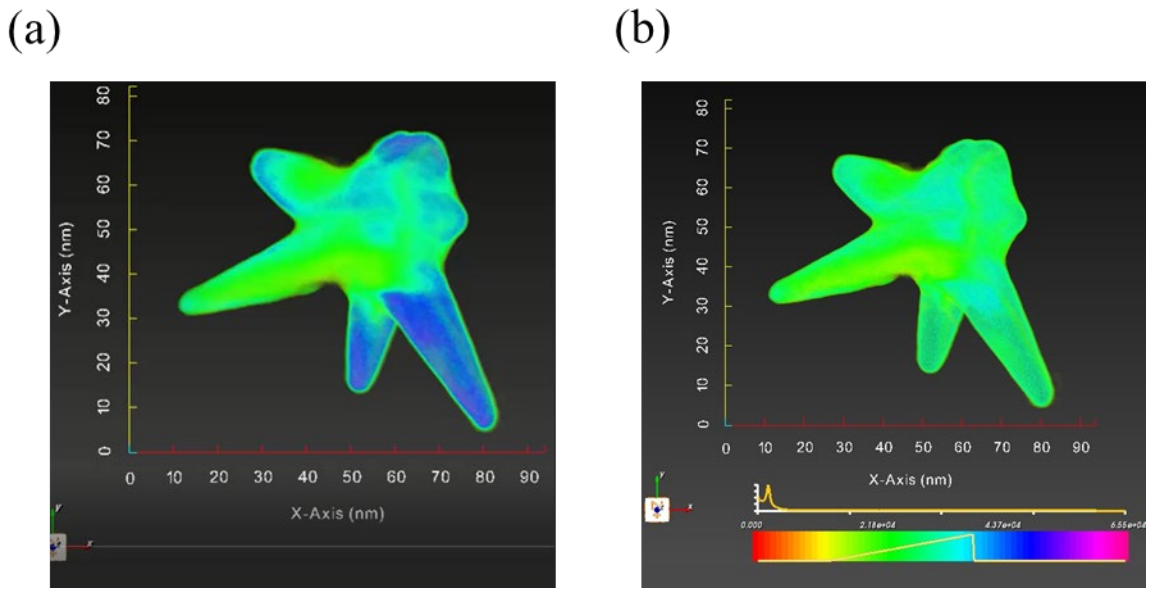

Fig. 7 Tomography of Au18Ag4; (a) overall view, (b) image with low-signal area extracted.

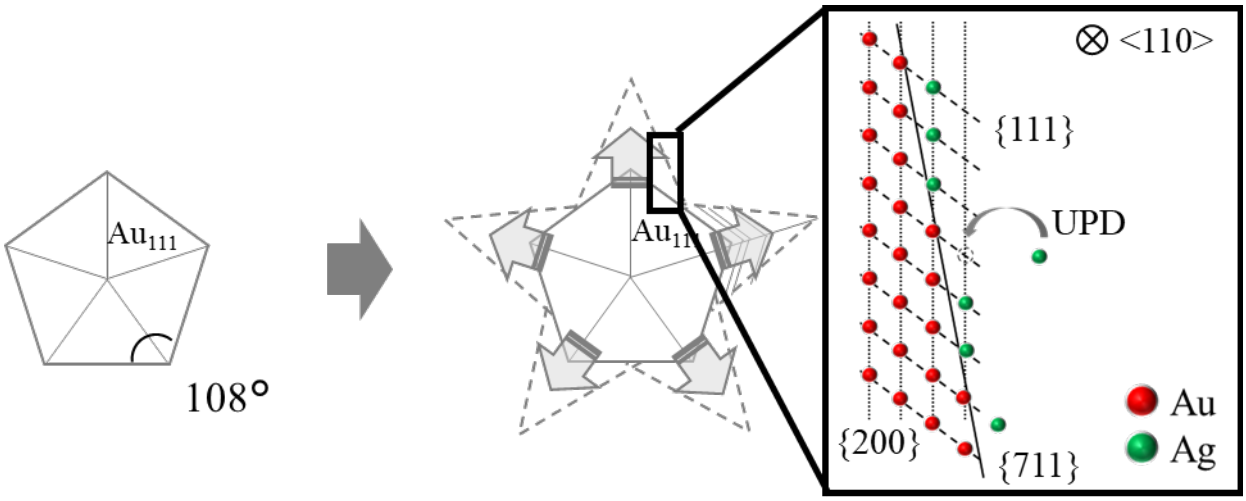

Fig. 8 Schematic diagram of the novel growth mechanism of star-shaped nanoparticles; red is Au atom and green is Ag.